

Characterization of electrowetting processes through force measurements

Nathan B. Crane, Pradeep Mishra, and Alex A. Volinsky

Department of Mechanical Engineering, University of South Florida, Tampa, Florida 33620, USA

(Received 25 August 2009; accepted 5 March 2010; published online 6 April 2010)

A new method of characterizing electrowetting is presented. In this method, the electrowetting actuation forces are measured rather than the contact angle. The forces on the liquid are measured by trapping a droplet between a flat nanoindenter tip and the test substrate. When voltage is applied to electrodes in the substrate, lateral and normal forces are exerted on the tip and measured by the nanoindenter transducer. Proper selection of the tip geometry permits direct prediction of the resulting in-plane lateral forces using analytical formulas derived from the Young–Lippmann equation. Experimental results show good agreement with both analytical and numerical predictions. Numerical modeling using SURFACE EVOLVER shows that the lateral forces are relatively insensitive to most alignment errors and that the analytical model is most accurate when the flat tip is close to the substrate. Evaporation of the test liquid can introduce modest errors in long measurements, but compensation methods are presented. As the droplet undergoes almost no movement, the fluid dynamics have minimal impact on the measured forces and transient electrowetting events are readily detected. Experimental results show significant response at frequencies up to 40 Hz. This setup is useful in measuring electrowetting responses at high speeds and in measuring system degradation processes. © 2010 American Institute of Physics.

[doi:10.1063/1.3373945]

I. INTRODUCTION

Electrowetting was first identified by Lippmann in 1857, but recent advancements have led to an explosion of potential applications.¹ This effect has been demonstrated for a wide range of liquids, including water, common solvents, and ionic liquids.^{2,3} Potential applications include digital microfluidics,^{4–7} responsive cooling,⁸ focusing lenses,^{9,10} and flexible displays.¹¹ Typically, the electrowetting liquid is contacted by one electrode from above while a second insulated electrode is located beneath the droplet as shown in Fig. 1. However, variations such as grounding the droplet from below and “floating drop” configurations¹² can provide simplified electrical connections and control for some applications. The incorporation of a dielectric layer between the liquid and electrodes to reduce electrochemical reactions is critical to many of these applications. However, the electrowetting response still involves complex coupling of electrical, chemical, fluid, and surface properties. As such, many aspects of electrowetting behavior are not yet fully understood. These include dielectric charging,^{13,14} asymmetric (polarity dependent) electrowetting responses,¹⁵ and saturation phenomena.^{16–18} The insulating dielectric layer is commonly coated with a thin hydrophobic coating (not shown).

Electrowetting can be addressed from various perspectives (thermodynamic, electrochemical, energy minimization, and electromechanical), but the electromechanical approach has been receiving increased attention.¹⁹ Still, contact angle measurement remains the predominant experimental method for investigating electrowetting phenomena. The equilibrium contact angle (θ_1) under an applied voltage can

be related to the thickness (δ) and dielectric constant (ϵ_0, ϵ_R) of the dielectric layer by the Young–Lippmann equation¹

$$\cos \theta_1 = \cos \theta_0 + \frac{\epsilon_0 \epsilon_r V^2}{2 \gamma_{lv} \delta}, \quad (1)$$

where V is the voltage applied between the substrate electrode and the droplet and θ_0 is the liquid’s contact angle without applied voltage (at $V=0$). The quantity $\epsilon_0 \epsilon_r V^2 / 2 \delta$ is simply the energy stored per unit area in a parallel plate capacitor so that the change in apparent energy of the droplet/substrate interface is equal to the capacitive energy storage. This relationship generally agrees with test data below a critical voltage referred to as the saturation voltage.

High speed measurements of contact angle are difficult to relate to the electrowetting response. When the droplet interface is in motion, the contact angle depends on both the fluid dynamics and electrowetting phenomena. Thus, the Young–Lippmann equation does not apply. Verheijen and Prins²⁰ developed an alternative approach to electrowetting characterization in which the capacitance between the drop and the substrate is measured. As the contact angle decreases, the droplet spreads, increasing the effective area of the capacitor. The resulting capacitance change can be correlated with the contact angle to provide highly repeatable measurements. However, during rapid changes, the measurement still depends on both fluid dynamics and electrowetting effects. Recent work has shown that dynamic effects significantly affect the shape of millimeter-scale droplets²¹ and even the saturation voltages¹⁷ over a large range of voltage frequencies.

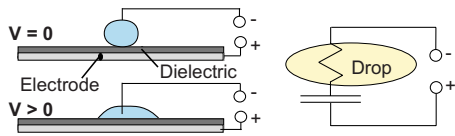


FIG. 1. (Color online) Illustration of basic electrowetting concept and the equivalent lumped-parameter circuit model.

This work considers force-based measurement of electrowetting. If the droplet is constrained from moving to an equilibrium position, a force will be applied to the constraint. This force can be measured and related to the electrowetting response. In the present work, the droplet is trapped between two flat surfaces, at least one of which is wetted by the fluid. The geometrical constraints on the droplet minimize the fluid motion during testing so that electrowetting changes are separated from fluid dynamics effects. Additionally, the electrowetting actuation forces are of more direct interest than contact angle in many electrowetting applications, particularly where electrowetting is used to move a droplet or something wetted by the droplet.^{22,23} By restraining movement of the three phases contact line, this approach may also provide new insights into electrowetting saturation.²⁴

Models of electrowetting forces (EWFs) have been developed previously using techniques from continuum electromechanics^{19,25,26} to atomistic simulations.²⁷ However, limited force measurements have been made. Some have focused on the performance of a specific device such as a microgripper.²³ The others are based on nanoscale measurements. For example, Guan *et al.*²⁸ used an atomic force microscope to measure EWFs of water condensate on polymethyl methacrylate as a function of applied voltage, and Chen *et al.*²⁹ measured the force of mercury wetting a carbon nanotube. These tests provide valuable information about nanoscale phenomena, but the results are difficult to extrapolate to microscale and mesoscale situations where most electrowetting applications are studied.

EWF measurements at a larger scale provide a valuable

means of assessing predictive force models, characterizing the dielectric layers, tracking their degradation over time, studying phenomena such as trapped charges, detecting electrochemical corrosion, and studying electrowetting response on textured surfaces. A measurement method that addresses these needs is described below and basic force relationships are developed. The sensitivity of the measurement system to key measurement parameters is then evaluated using numerical models. Finally, experimental measurements from the force measurement system are reported for steady and dynamic inputs.

II. EWF MEASUREMENT APPARATUS

The EWF is measured using a modified Hysitron Triboindenter nanoindentation apparatus.³⁰ The commercial nanoindenter has micronewton force resolution in two axes (normal and lateral). Figure 2(a) illustrates how it can be adapted for EWF measurement by attaching a flat $9 \times 9 \times 0.15$ mm³ glass plate to a custom tip that is parallel to a test substrate. For optimal alignment of the glass plate to the substrate, the glass plate can be attached to the indenter by adhesive using the substrate as an alignment guide. The nanoindenter has calibrated optical alignment system that permits positioning of the plate center to within ~ 1 μ m and angular alignment of the plate edges with the electrode edges to within 0.25° .

The test substrate contains one or more electrodes covered by a dielectric layer as illustrated in Fig. 2(a). A thin hydrophobic coating can be applied if necessary to create a hydrophobic top surface. Tests are performed by placing a droplet on the substrate and lowering the glass plate until it is entirely wet with the test solution. The glass surface was chosen for testing aqueous solutions because in general, they wet the glass well. Once the droplet is sandwiched between the substrate and the glass plate, it will move with the glass plate. The droplet should be positioned so that it bridges the gap between the electrodes.

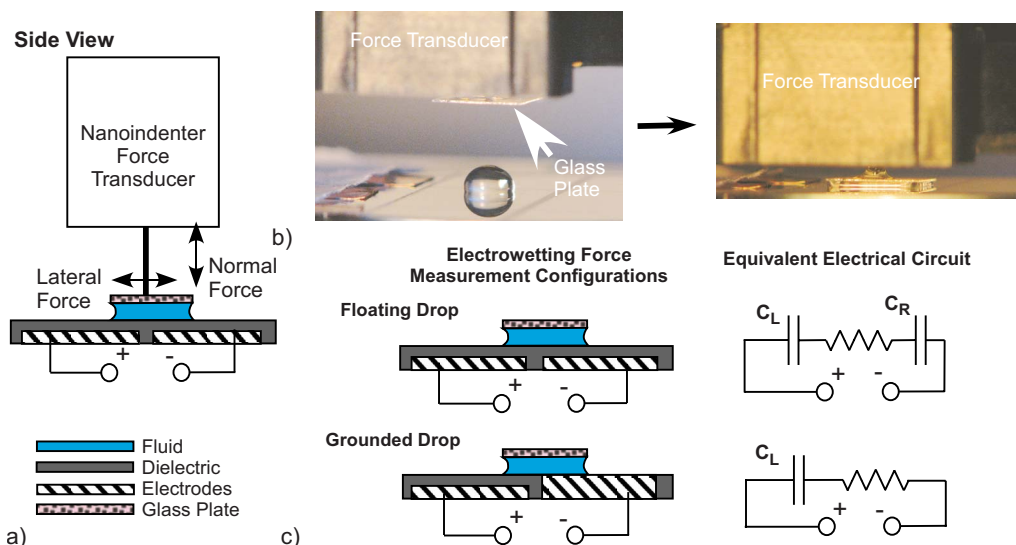


FIG. 2. (Color online) Illustration of the EWF measurement method. (a) Schematic representation of the measurement setup. (b) Photos of the glass plate attached to the force transducer before and after contacting the liquid drop. (c) Comparison of substrate setup and lumped-parameter circuit models for two common EWF test modes.

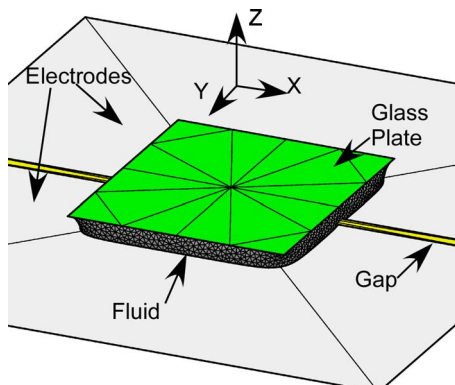


FIG. 3. (Color online) Illustration of basic SURFACE EVOLVER model geometry.

While many electrical configurations of the substrate are possible, two of primary interest, floating drop and grounded drop, are shown in Fig. 2(c). The EWF model can be developed using the lumped parameter electrical model illustrated in the figure. As the height of the glass plate above the substrate decreases, the contact region of the test solution on the substrate approaches the area and shape of the glass plate as seen in Fig. 2(b). Under the floating drop arrangement, the droplet creates two series capacitors with the two electrodes under the dielectric. The area of each capacitor can be calculated as a function of the offset (y) of the plate's center from the electrode boundary. Given the gap (g) between adjacent electrodes and the length of the glass plate (L), the left and the right areas (A_L , A_R) are given by

$$A_L = L(L - g - 2y)/2, \quad (2)$$

$$A_R = L(L - g + 2y)/2, \quad \text{for } -(L - g)/2 < y < (L - g)/2.$$

Modeling the droplet interfaces as two parallel plate capacitors with capacitance (C_L , C_R), the total capacitive energy (E_{cap}) is given by

$$E_{\text{cap}} = (C_L V_L^2 + C_R V_R^2)/2 = \epsilon_0 \epsilon_r (A_L V_L^2 + A_R V_R^2)/2\delta, \quad (3)$$

$$V_L = V_{\text{tot}} A_R / (A_L + A_R), \quad V_R = V_{\text{tot}} A_L / (A_L + A_R), \quad (4)$$

where V_L and V_R are the voltages on the left and right sides, respectively. The lateral force (F_y) in the system can be found by combining Eqs. (1)–(3) and differentiating the energy with respect to the displacement so that

$$E = \frac{\epsilon_0 \epsilon_r L V_{\text{tot}}^2}{2\delta} \left(\frac{L - g}{4} - \frac{y^2}{L - g} \right), \quad (5)$$

$$F_y = dE/dy = - \frac{\epsilon_0 \epsilon_r L V_{\text{tot}}^2}{(L - g)\delta} y. \quad (6)$$

In the grounded droplet configuration, the lumped parameter model consists of a single capacitor so that the voltage at the interface is the total voltage applied. The force is then

$$F_y = - \epsilon_0 \epsilon_r L V_{\text{tot}}^2 / \delta. \quad (7)$$

Note that while the contact angle depends on the liquid-vapor surface energy (γ_{lv}), the predicted force at a particular

TABLE I. Surface evolver model parameters.

Variable	Value
Gap width (g)	0.5 mm
Surface energy (γ_{lv})	0.072 J/m ²
Liquid/substrate contact angle (θ_o)	110°
Liquid/measurement plate contact angle	20°
Plate side length (L)	9 mm
Dielectric constant (ϵ_r)	2.1
Dielectric thickness (δ)	2.1 μ m
Voltage (V)	100 V
Liquid volume (V_f)	40.5 μ l
Plate height above the substrate (h)	500 μ m

voltage is independent of the surface energies as long as the Young–Lippmann equation holds true ($V_{\text{tot}} < V_{\text{sat}}$).^{1,16} Actuation liquids with higher saturation voltages will produce higher peak forces, but at lower voltages, the EWF is predicted to be independent of the electrowetting liquid used. Exceptions as seen in Fig. 10(a) are believed to be due to material and dynamic effects such as ion transport into the dielectric layers that are not included in this model. The EWF method can be used to study these phenomena.

The above model assumes that the liquid interface with the substrate matches both the shape and location of the glass plate. The validity of this assumption was evaluated by modeling the floating droplet configuration using version 2.26 of SURFACE EVOLVER.³¹ For this analysis, gravity and surface tension contributions were included. The equilibrium surface is found by a gradient-based solution of the shape that minimizes the total energy. In the model (Fig. 3), the interfacial energy is calculated using the Young–Lippmann equation based on the contact area of the fluid over each electrode. Similar methods were used by Lienemann *et al.*³² to simulate droplet motion by electrowetting. The forces applied to the top plate are calculated numerically from the derivative of the system energy with respect to the displacement of the plate in the direction of interest ($F_j = dE/du_j$, where u_j is a unit vector in the direction of interest).

The test configuration parameters are summarized in Table I. The SURFACE EVOLVER models closely match the results predicted by Eq. (5) for the grounded and floating droplet cases at small tip/substrate height (h). Figure 4 shows results for the floating droplet case. As the tip height above the substrate increases, the force- y -offset relationship remains linear, but the slope decreases. This is due to deviations from the assumption that the droplet shape matches the plate shape at larger tip heights.

III. FORCE SENSITIVITY TO ALIGNMENT ACCURACY

Equations (1)–(5) are based on the alignment of the incenter plate parallel to the substrate and a “small” height of the plate above the substrate. However, practical implementation of these methods requires an assessment of the sensitivity of the measurements to the alignment accuracy.³³ SURFACE EVOLVER models were used to examine impact of various errors on the force applied to the tip. Rotations were applied to the plate in the SURFACE EVOLVER models using

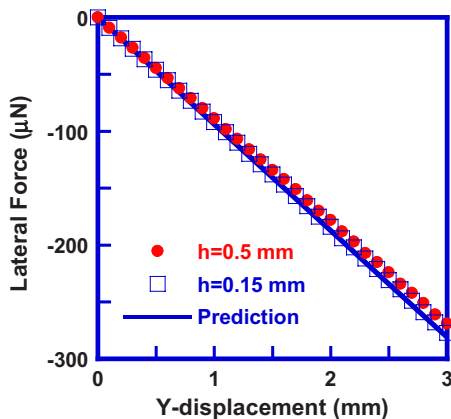


FIG. 4. (Color online) Analytical and SURFACE EVOLVER predictions of the EWF as a function of displacement. The accuracy of the simple model decreases as the plate height (h) decreases.

the coordinate system shown in Fig. 3 and the force was calculated as a function of rotation for a 3 mm offset. The fluid volume (V_f) is set to the projected volume below the perfectly aligned plate ($V_f = hL^2$). For each rotation type, the analysis began with the minimum angle error (-5°). The plate was rotated in 0.25° increments to the maximum error and then reduced back to the minimum error. The force difference between increasing and decreasing angles is a function of the convergence accuracy of the SURFACE EVOLVER models with convergence errors less than 1% of the total force. The results are summarized in Fig. 5.

Normal forces show large sensitivity to alignment errors in all axes except the z -axis. Thus the normal force data provide little useful information in practice. However, the lateral forces are relatively insensitive to angular misalignments of all types. Rotations around the y -axis and z -axis introduce force errors of approximately 1% at 5° . The force errors are much more significant for x -axis rotations. Positive rotational errors (smaller plate heights on the small area, high voltage side) produced larger errors (4.4% at $+5^\circ$) than negative rotations (1.9% at -5°). X and y -axes alignment errors can be maintained well below five degrees by using the substrate as an alignment aid. Similar alignment accuracy in the z -axis can be achieved by optically verifying the alignment of the glass plate to the machine axes before bonding it to the tip.

While the initial analysis assumes that the liquid volume is the same as the projected volume, this may be difficult to

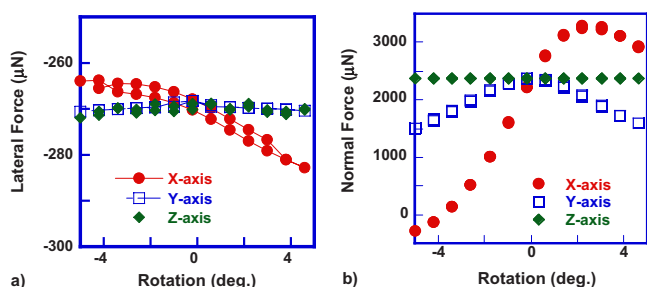


FIG. 5. (Color online) Variation in lateral and normal forces with rotational misalignment errors about each axis as predicted by SURFACE EVOLVER models. Lateral forces are relatively insensitive to alignment errors.

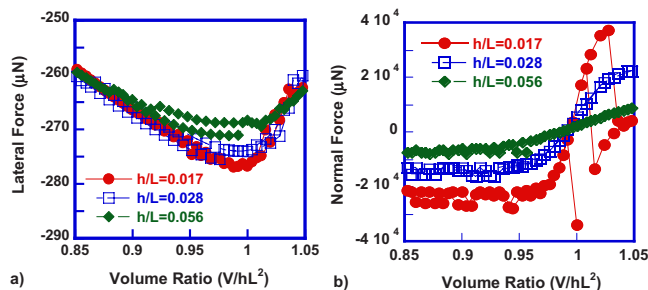


FIG. 6. (Color online) Variation in normal and lateral forces with liquid volume as predicted by SURFACE EVOLVER models. Larger heights show less sensitivity to changes in the liquid volume in both lateral and normal forces. Normal forces are much more sensitive to liquid volume than are lateral forces.

achieve in practice due to inaccuracy in dispensing droplets and change in the liquid volume over time through evaporation. The impact of variable liquid volume was analyzed using the SURFACE EVOLVER models at three different values of the height ratio (h/L). For each height ratio, the volume ratio (V_f/hL^2) was decreased from 1.0 to 0.85, increased to 1.05, and then decreased back to 1.0 to evaluate hysteresis and model convergence. The results are summarized in Fig. 6.

As in the previous case, the lateral forces are less sensitive to variations in volume than the normal forces. The lateral forces decrease as much as 6% from their peak magnitude as the volume ratio decreases to 0.85 (15% decrease). For $h/L=0.017$, there is significant hysteresis in the normal forces for volume ratios above 1.0 due to the formation of a large protrusion of liquid at high volume ratios. However, despite this large change in shape, the lateral forces remain very stable. The largest lateral forces are seen for a volume ratio at or slightly below unity. These data suggest that testing should be performed at volume ratios near unity. Of note, the large height ratios (variation $<5\%$ for $h/L=0.056$) are less sensitive to the evaporation effects than small height ratios (variation $\sim 10\%$ for $h/L=0.017$). As evaporation will decrease the volume of many test liquids during testing, large height ratios are preferred for their decreased sensitivity to the declining liquid volume. While this large height ratio slightly decreases lateral force (Fig. 4), the decreased sensitivity to droplet volume is a significant advantage.

During longer tests, the drift in the lateral forces due to evaporation may prevent accurate detection of changes in the electrowetting behavior. The evaporation rate of an exposed water droplet hanging from a flat tip was measured as $0.3 \mu\text{l}/\text{min}$. During EWF testing, the exposed surface area is much smaller ($<25 \text{ mm}^2$) than during the evaporation test ($>81 \text{ mm}^2$). Thus, a $50 \mu\text{l}$ drop is expected to lose less than 1% of its volume during a 5 min test.

When long test times or fluids with higher evaporation rates are required, additional measures should be considered. Improved stability can be achieved by adjusting the tip height during testing to maintain a constant volume ratio as the droplet evaporates. Figure 7 shows that this dramatically reduces the variation in the lateral forces with changing liquid volume. A 25% reduction in liquid volume resulted in just 1% change in the lateral force when the volume ratio was maintained constant. As the normal forces go to zero

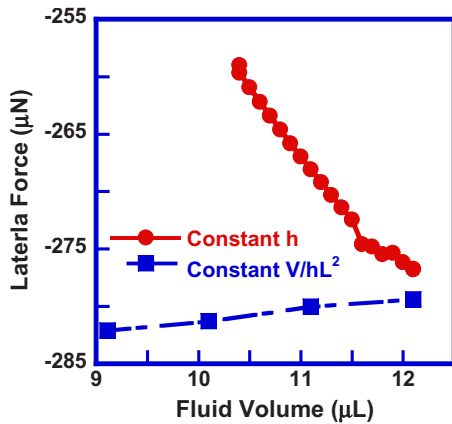


FIG. 7. (Color online) SURFACE EVOLVER model results comparing lateral forces with liquid volume for constant plate height and a constant liquid volume/projected volume ratio. The constant ratio produces more stable force measurements.

when the volume ratio approaches unity, the normal force could be used as a control signal to adjust the tip height during testing. With height adjustments to maintain a constant volume ratio, hour long tests appear to be feasible. Further improvements are possible by using a saturated atmosphere or submerging the glass plate in a second immiscible liquid to reduce the evaporation rate. Similar arrangements have been made previously for nanoindentation in liquids.³⁴

IV. EXPERIMENTAL EWF DATA

Test structures were prepared on silicon wafers with a 500 nm layer of thermal oxide. A 300-nm-thick aluminum film was deposited by sputtering and patterned photolithographically via wet etching. CYTOP™ 809M, a fluoropolymer produced by Asahi Glass company, was spin coated over the patterned wafer in two layers. After the first coating of CYTOP™ wafers were baked at 90 °C for 30 min. Then a second layer of CYTOP™ was spin coated and final baking was done at 150 °C for 1 h. The thickness of the CYTOP™ films was measured by a step profilometer with typical thickness of the two CYTOP™ layer ranging from 2 to 2.2 μm. Electrical connections to the aluminum electrodes were made using conductive copper tape.

Prepared substrates were mounted on the Hysitron Triboindenter test platform. A 55 μl droplet of a 1 mM Na₂SO₄ solution was dispensed on the substrate with a micrometer syringe. Larger droplets were used than in the simulations to allow for drop evaporation during testing. The glass plate was moved into the test position (typically 3 mm offset from the electrode gap) and lowered until the entire glass plate surface was wet with the salt solution. Voltage was then applied to the substrate electrodes while the force was measured using the Hysitron transducer. dc voltages were applied using a Matsusada RG-360–0.2 power supply. Dynamic electrical inputs were amplified from a function generator using a Matsusada AMS-1B30 amplifier.

In a series of tests, increasing dc voltages were applied to the substrate electrodes while the resulting forces were recorded. From 50 to 110 V, the maximum lateral force compares well with predictions from Eq. (5) and Surface Evolver

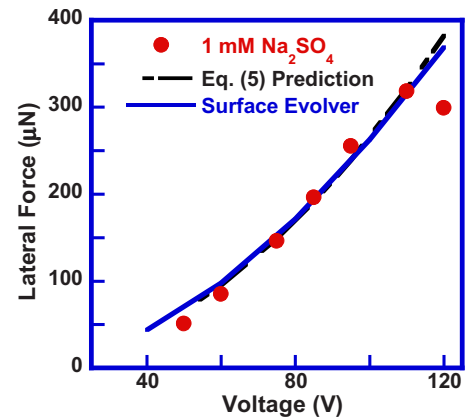


FIG. 8. (Color online) Comparison of measured peak lateral forces with analytical and numerical predictions.

models as seen in Fig. 8. The measurement method is sensitive to defects in the dielectric layer.³⁵ This is helpful in studying the dielectrics, but the current CYTOP™ dielectric layers frequently contain local defects that introduce force deviations preventing accurate determination of the method repeatability.

This peak force data give information comparable to the contact angle data, but the time-response data provide clues to the nature of the degradation mechanisms. Figure 9(a) shows the force response data and applied voltage for the above test case versus time. The data show a fast response time ($\ll 1$ s) and a residual force after removal of the applied voltage. This residual force could be related to charge trapping in the dielectric layer. It also captures a sharp change in the applied force approximately 1 s after the application of 110 V [Fig. 9(b)]. After 1.2 s, the force suddenly dropped from 349 to 318 μN in the 0.05 s interval between data points, after which a steady decline in force ensued. When 120 V was subsequently applied, the force was well below the predicted value (Fig. 8). The sharp drop in force and subsequent change in behavior suggests a sudden local failure in the dielectric coating well below the manufacturer-reported breakdown field. The fluid on the dielectric substantially reduces the dielectric breakdown fields relative to dry tests.³⁶ Transient spikes have been seen with many test liquids and are associated with electrode corrosion. Depending on the electrolyte, voltage polarity, and dielectric layer quality, the forces may increase, decrease, or remain unchanged with prolonged voltage exposure. The high time resolution of

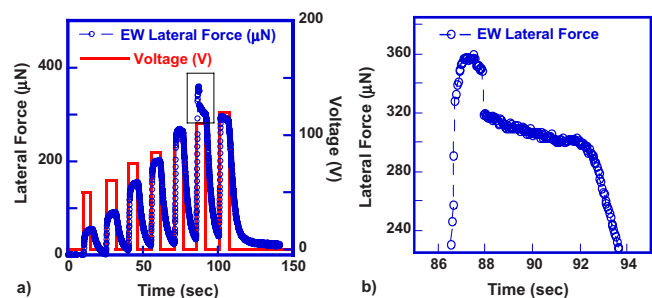


FIG. 9. (Color online) EWF lateral force data for 1 mM Na₂SO₄ solution. (a) Response to a series of dc voltage pulses. (b) Plot of peak EWF data for the 110 V pulse.

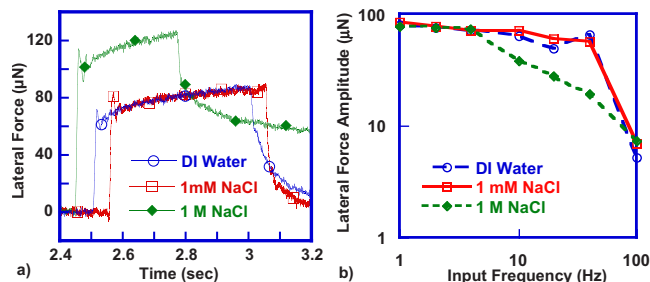


FIG. 10. (Color online) (a) Lateral force response to a step from 0 to 75 V shows some overshoot followed by a decaying oscillation for three different liquids. (b) Frequency response data for EWF lateral forces for three different liquids.

these data provides opportunity for new insight into the electrowetting response and its degradation. Additional insight could be obtained by integrating EWF with current measurements similar to Raj *et al.*³⁶

The EWF response at high frequencies was measured to evaluate the frequency response limits of the EWF method. Using the 9×9 mm² plate with a 55 μ l droplet, 75 V square pulses were alternated with zero voltage time periods of equal length at varying frequencies. In contrast, typical work with ac excitations use zero mean voltage waveforms and high frequencies (>1 kHz) to minimize migration of charged species into the dielectrics.³⁶ Figure 10(a) shows data from a 1 Hz pulse for three different liquids [de-ionized (DI) water, 1 mM NaCl, and 1M NaCl]. The initial response to the step input is typical of a damped second order system with an overshoot and decaying oscillation. The oscillation frequency was estimated by measuring the distance between the first two peaks. Average frequencies were 41, 52, and 55 Hz for DI water, 1 mM NaCl, and 1M NaCl, respectively. The frequency differences may be related to the variation in fluid conductivity and/or liquid volume ratios at the time of the test. Figure 10(b) summarizes the peak to peak amplitudes measured for each liquid as a function of frequency when subject to the alternating 0 and 75 V inputs. The high salt concentration (1M NaCl) showed a decreased response above 4 Hz, but the lower salt concentration fluids (DI water and 1 mM NaCl) showed good response out to 40 Hz. When the transducer was tapped with the plate attached, the first vibration mode was measured as 285 Hz. This suggests that the transducer response is not limiting the EWF measurement. Further study is required to identify the parameters which limit the EWF frequency response in the test system.

These data show the complexity of electrowetting systems. While basic models suggest that the response should be independent of the liquid used, the results clearly vary with the liquid. A likely explanation for the differences is in the transport of the dissolved ions into the CYTOP™ dielectric layer under the applied electric field. As the ions diffuse inward, the effective field at the fluid/dielectric interface can be reduced, generating lower EWFs for a given applied voltage.^{13,14} However, upon removal of the applied voltage, the trapped charges dissipate very slowly creating a large residual force as seen in Fig. 10(a) for the 1M NaCl solution. This effect would be largest for higher ionic concentrations as observed here and would increase over time. As the fre-

quency tests were done sequentially on the same sample, this could have caused an apparent decrease in the force response at higher frequencies as seen in Fig. 10(b). On the other hand, when imperfections in the dielectric layer permit some current to flow through the fluid, higher ionic conductivities would reduce the voltage drop in the fluid. This in turn would create a large voltage drop at the interface so that the applied force could increase with ionic conductivity as was observed in the initial voltage application [Fig. 10(a)]. The EWF method provides a valuable tool to help clarify the contributions of these and other effects to the performance of electrowetting systems.

V. CONCLUSIONS

A method for measuring the force applied to a liquid droplet by the electrowetting effect has been presented. The method uses a custom flat tip attached to a commercial nanoindenter with a two-axis force transducer. This system provides a high resolution force measurement with a fast response time. The EWF measurement method is shown to have low sensitivity of the lateral force to alignment and liquid volume errors. In contrast, the normal force is very sensitive to these errors making it very difficult to interpret normal force data. Thus, analysis focuses on the lateral force data. The geometry of the system permits straightforward estimates of the force from analytical predictions. These predictions show good agreement with numerical models and experimental data. As this method minimizes liquid motion, it permits close examination of the electrowetting phenomena during dynamic events. This method will be useful in detecting degradation in the electrowetting response over time and identifying the degradation mechanisms. It could also be used to identify mechanisms for increasing the speed of droplet actuation.

ACKNOWLEDGMENTS

Vivek Ramadoss made valuable contributions to this work through the initial studies that he performed. These served as a foundation for the present paper. Nathan Crane would like to acknowledge support from NACE International, the University of South Florida Research Education Initiative Program under Grant No. FMMD04, and from NSF under Grant No. CMMI-0927637. Alex Volinsky would like to acknowledge support from the National Science Foundation under Grant No. CMMI-0600266. The authors would like to thank Hysitron, Inc. for providing blank tips and useful discussion.

¹F. Mugele and J. C. Baret, *J. Phys.: Condens. Matter* **17**, R705 (2005).

²D. Chatterjee, B. Hetayothin, A. R. Wheeler, D. J. King, and R. L. Garrell, *Lab Chip* **6**, 199 (2006).

³S. Millefiorini, A. H. Tkaczyk, R. Sedev, J. Efthimiadis, and J. Ralston, *J. Am. Chem. Soc.* **128**, 3098 (2006).

⁴P. Paik, V. K. Pamula, M. G. Pollack, and R. B. Fair, *Lab Chip* **3**, 28 (2003).

⁵S. K. Cho, H. J. Moon, and C. J. Kim, *J. Microelectromech. Syst.* **12**, 70 (2003).

⁶Y. Zhao and S. K. Cho, *Lab Chip* **7**, 273 (2007).

⁷P. Y. Chiou, H. Moon, H. Toshiyoshi, C. J. Kim, and M. C. Wu, *Sens. Actuators, A* **104**, 222 (2003).

- ⁸K. Mohseni and E. S. Baird, *Nanoscale Microscale Thermophys. Eng.* **11**, 99 (2007).
- ⁹S. Kuiper and B. H. W. Hendriks, *Appl. Phys. Lett.* **85**, 1128 (2004).
- ¹⁰L. Dong, A. K. Agarwal, D. J. Beebe, and H. R. Jiang, *Nature (London)* **442**, 551 (2006).
- ¹¹R. A. Hayes and B. J. Feenstra, *Nature (London)* **425**, 383 (2003).
- ¹²C. G. Cooney, C. Y. Chen, M. R. Emerling, A. Nadim, and J. D. Sterling, *Microfluid. Nanofluid.* **2**, 435 (2006).
- ¹³H. J. J. Verheijen and M. W. J. Prins, *Langmuir* **15**, 6616 (1999).
- ¹⁴M. K. Kilaru, J. Heikenfeld, G. Lin, and J. E. Mark, *Appl. Phys. Lett.* **90**, 212906 (2007).
- ¹⁵S. K. Fan, H. P. Yang, T. T. Wang, and W. Hsu, *Lab Chip* **7**, 1330 (2007).
- ¹⁶A. Quinn, R. Sedev, and J. Ralston, *J. Phys. Chem. B* **109**, 6268 (2005).
- ¹⁷K. L. Wang and T. B. Jones, *Appl. Phys. Lett.* **86**, 054104 (2005).
- ¹⁸K. H. Kang, *Langmuir* **18**, 10318 (2002).
- ¹⁹T. B. Jones, *Mech. Res. Commun.* **36**, 2 (2009).
- ²⁰H. J. J. I. Verheijen and M. W. J. I. Prins, *Rev. Sci. Instrum.* **70**, 3668 (1999).
- ²¹S. H. Ko, H. Lee, and K. H. Kang, *Langmuir* **24**, 1094 (2008).
- ²²I. Moon and J. Kim, *Sens. Actuators, A* **130–131**, 537 (2006).
- ²³A. Vasudev and J. Zhe, *Appl. Phys. Lett.* **93**, 103503 (2008).
- ²⁴A. I. Drygiannakis, A. G. Papanthanasidou, and A. G. Boudouvis, *Langmuir* **25**, 147 (2009).
- ²⁵E. Baird, P. Young, and K. Mohseni, *Microfluid. Nanofluid.* **3**, 635 (2007).
- ²⁶E. S. Baird and K. Mohseni, *Nanoscale Microscale Thermophys. Eng.* **11**, 109 (2007).
- ²⁷A. Kutana and K. P. Giapis, *Nano Lett.* **6**, 656 (2006).
- ²⁸L. Guan, G. Qi, S. Liu, H. Zhang, Z. Zhang, Y. Yang, and C. Wang, *J. Phys. Chem. C* **113**, 661 (2009).
- ²⁹J. Y. Chen, A. Kutana, C. P. Collier, and K. P. Giapis, *Science* **310**, 1480 (2005).
- ³⁰N. B. Crane, A. A. Volinsky, V. Ramadoss, M. Nellis, P. Mishra, and X. Pang, *Mater. Res. Soc. Symp. Proc.* **1052**, DD8.1 (2007).
- ³¹K. Brakke, *Exp. Math.* **1**, 141 (1992).
- ³²J. Lienemann, A. Greiner, and J. G. Korvink, *IEEE Trans. Comput.-Aided Des.* **25**, 234 (2006).
- ³³V. Ramadoss and N. B. Crane, Proceedings of the 2008 ASME International Mechanical Engineering Congress, 2008.
- ³⁴M. Pendergast, A. A. Volinsky, X. Pang, and R. Shields, *Mater. Res. Soc. Symp. Proc.* **1085E**, T5.10 (2008).
- ³⁵N. B. Crane, A. A. Volinsky, P. Mishra, A. Rajgadkar, and M. Khodayari, *Appl. Phys. Lett.* **96**, 104103 (2010).
- ³⁶B. Raj, M. Dhindsa, N. R. Smith, R. Laughlin, and J. Heikenfeld, *Langmuir* **25**, 12387 (2009).